Twinkling Pixels: Random Telegraph Signals at Reset Gate Edge

Bedabrata Pain, Bruce Hancock, Chao Sun, and Chris Wrigley
Jet Propulsion Laboratory, California Institute of Technology
4800 Oak Grove Drive, Pasadena, CA 91109
Phone: 818-354-8765; Fax: 818-393-0045; Email: bpain@jpl.nasa.gov

As a result of a significant lowering of dark current in CMOS imager pixels, as well as the introduction of deep sub-μm processes, several secondary dark current sources are becoming detectable, often greatly impacting the spatial distribution of these two metrics. While modal values of dark current have fallen below 50 pA/cm^2, the spatial distribution is far from gaussian – the tail of the distribution easily extending ten times larger than the modal value. There are several reasons for the dark current tail - the presence of isolated metallic impurities, electric field induced dark current enhancements, a distribution of the spatial location of the metallic impurities near the offending junction, hot electron effects being some of the causes [1,2,3].

Usually, the dark current is found to be the results of a stationary statistical process – i.e. repeated measurements yield statistically similar results. In this paper, we report the results from measurements on a 512x512 format imager that had isolated pixels exhibiting non-stationary characteristics. Non-stationarity was observed in form of pixels whose dark current would vary from frame to frame – giving rise to a twinkling effect.

Non-stationary behavior in CMOS imager pixels have been previously reported, and is linked to random telegraph signals (RTS) that are generated within the source-follower channel [4,5,6,7,8,9]. RTS is shown to be a major source of temporal noise in CMOS imager pixels implemented in a deep sub-micron technology [10]. However, in the image sensor we evaluated, the twinkling behavior was not due to RTS in the source-follower, but was directly linked to the sense node dark current.

Figure 1a shows a "3T" pixel schematic and the schematic cross-section of the sense node. It consists of a sense node buffered by a switched source-follower, the source-follower itself being the source of the reset FET. The sense node is reset by momentarily pulsing the reset line (RST) to V_H. During exposure, the reset FET is shut off by returning the reset line to V_L, and charge accumulated on the sense node. The pixels (with 12 μm pixel pitch) were implemented in a 0.15 μm 1 poly 4 metal CMOS process.

To better investigate the twinkling phenomena, we collected data from the twinkling pixels using the timing pattern shown in figure 2. First, the pixel was reset, and the reset signal was sampled. The reset FET was then turned, and its gate was held at V_L=0.5V. The pixel output (corresponding to the sense node potential V_S) was then sampled in regular intervals of 7.8 msec upto a maximum of 2 sec, after which the pixel was reset, and the experiment was repeated.

Figure 3 shows the results of multiple runs of a twinkling pixel near room temperature. Each data point represents the difference between the actual output and the reset level of the pixel for that run. Figure 3 shows several interesting phenomenon. First, for most of the runs (70%), the dark signal accumulations are identical, reaching ~400 mV in 2 sec, corresponding to ~ 0.8 nA/cm^2 leakage current. Secondly, the dark signal evolution is decidedly non-linear in time. Thirdly, during several runs, the dark current accumulation exhibits a completely different temporal dependence. In some cases, it starts off at a high rate, and slows down towards the end of the cycle, and at other times, it makes abrupt transitions in the middle of a cycle.

This seemingly strange voltage change at the sense node makes more sense once we take the derivative of the voltage with time. This yields the sense node leakage current (with appropriate conversion factors applied). Figure 3 shows the extracted leakage current plotted against the sense node differential voltage (0V on the x-axis is equivalent to the diode reset potential of ~1.5V). The resultant graph shows the reverse-bias leakage characteristics of a diode, whose leakage is, on one hand, voltage dependent, and on the other hand, exhibits two distinct states – a low and a high current, with random transitions between one to the other. Modulation of the leakage current due to random transitions manifests as twinkling. About 6% of the pixels were found to exhibit the twinkling behavior.

The high-state leakage current can be modeled as trap-assisted-tunneling (TAT), with the tunneling field being

proportional to the voltage difference between the potentials at the off-state reset gate (V_L) and the sense node (V_S). The extracted dark current fits the model [11]:

$$I_d = I_{fixed} + \alpha \cdot \exp\left[\frac{V_{RST} - V_S - V_L}{V_x}\right]^2$$

where I_{fixed} is the fixed current, α is the proportionality constant, V_{RST} is the reset voltage on the diode, V_L is the reset gate voltage, and V_x is the field-threshold voltage. At low V_S (small back-bias), the dark signal is small and linear, since the field-effect is minimal. But, as V_S increases (the sense node potential is closer to the reset potential), the leakage current increases significantly, and exhibits much larger dependence on the field.

Figure 4 shows the measured dark current (low state) for different bias conditions of the source-follower and sampling times (sampling period is fixed). No difference was found with the variation of sampling times, whereas the difference between the two curves corresponding to two different source-follower bias currents is entirely due to source-follower gain variation. In either case, figure 4 indicates that the source-follower operating conditions have no effect on the sense node leakage, ruling out hot-electron related effects.

The random change in dark current from one state to another can be postulated to be a result of an oxide trap changing its state. When the trap is filled, the net electric field seen by the sense node is smaller, and the dark current is lower. The generation mechanism is more of thermal origin. Conversely, when the trap is empty, the electric field is high, and the dark current is high and is due to trap-assisted-tunneling. Further evidence of this phenomenology comes from the fact that the activation energies of the high and low dark currents are widely different: near mid-gap (0.51 eV) for the low current state, and much lower (0.3 eV) and therefore more field-dependent for the high current state. Since the dark current in the high state depends not on the absolute value of V_s or V_L but on the difference between the two, it is likely that these traps are located in the LDD region of the reset FET, and not at the channel.

The rate of twinkling is also temperature dependent, the transitions slowing down as the temperature is reduced. Figure 5 shows the Arrhenius plot of the capture and emission rates of the bimodal sense node dark current. Data indicates the emission and capture are governed a thermal process with the activation energies being 0.12 eV and 0.39 eV respectively.

The number of twinkling pixels as well as the level of twinkling was reduced by reducing the electric field in the LDD region. With the reduced electric field, the trap state had little effect on the electric field seen by the sense node, resulting in suppression of dark current generation by trap-assisted tunneling, and hence suppression of large changes in dark current. The number of twinkling pixels reduced to less than 0.007% following electric field optimization.

Acknowledgments:

This research was carried out at the Jet Propulsion Laboratory, California Institute of Technology, and was sponsored by United States Space Missile Command and United States Missile Defense Agency through an agreement with the National Aeronautics and Space Administration.

References:

1. K. Yamaguchi et al., *IEEE Trans. Electron Devices*, vol. 46, pp. 1159-1165, 1999.
2. H. Kwon et al., *IEEE Trans. Electron Devices*, vol. 51, pp. 178-184, 2004.
3. B. Pain et al., *Proc. Workshop on CCD/AIS*,2005.
4. K.M. Findlater et al., *Proc. SPIE*, vol. 5251, pp 187-195, 2004.
5. C. Leyris et al., *Proc. SPIE*, vol. 5844, pp 41-51, 2005.
6. J. Janesick et al, *Proc. SPIE*, vol. 6276, pp. 99-108, 2006.
7. G.V. Groeseneken et al., *IEEE Trans. Electron Devices*, vol. 43, pp. 940-948, 1996.
8. E. Simoen et al, *IEEE Trans. Electron Devices*, vol. 39, pp. 422-429, 1992.
9. Y. Shi et al., *Semicond. Sci. Technol*., vol 16, pp 21–25, 2001.
10. X. Wang et al., *Tech. Digest Intl. Electron Dev. Meeting*, 2006.
11. G.A.M. Hurkx et al., *IEEE Trans. on Electron Devices*, vol. 39, pp. 331-338, 1992.

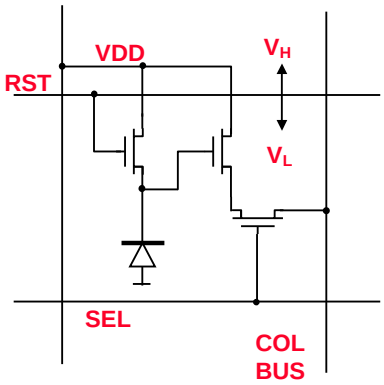

Figure 1a: Pixel schematic

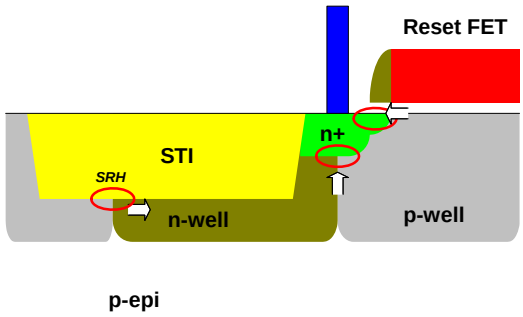

Figure 1b: Schematic cross-section

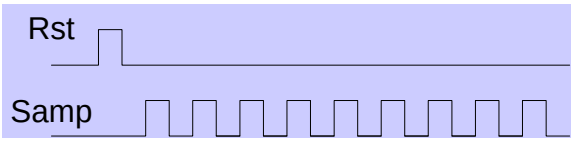

Figure 2: Timing diagram used for data collection

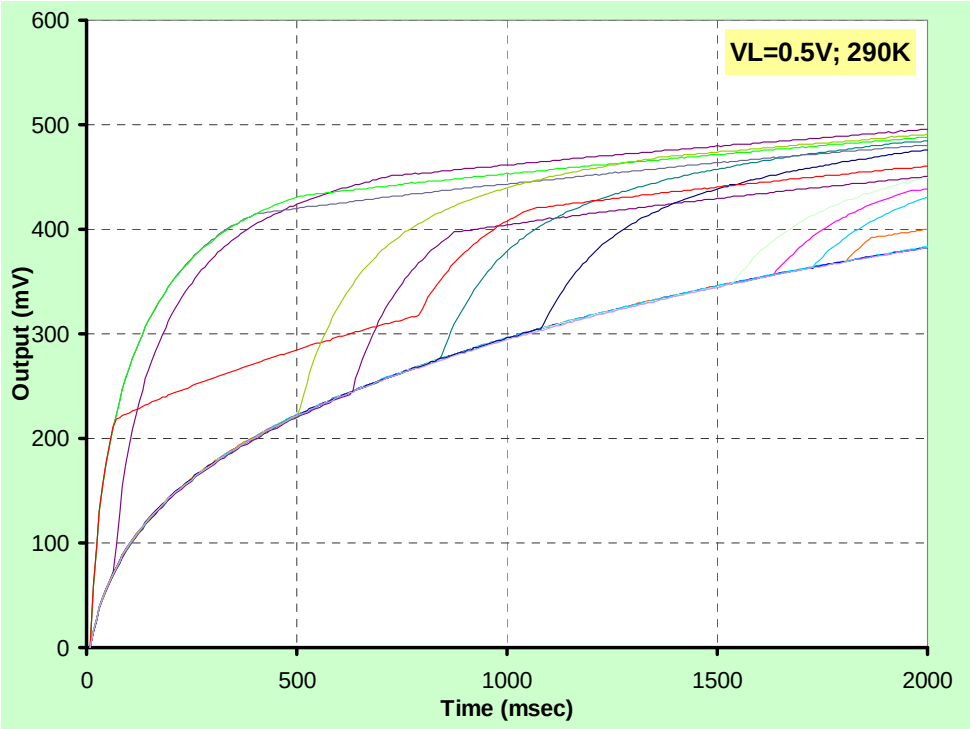

Figure 3: Measured data for two different source followe bias currents

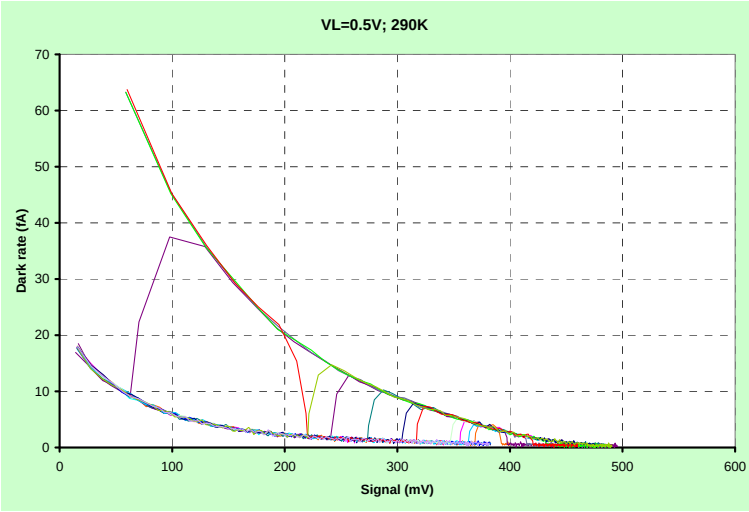

Figure 3: Measured data for two different source followe bias currents

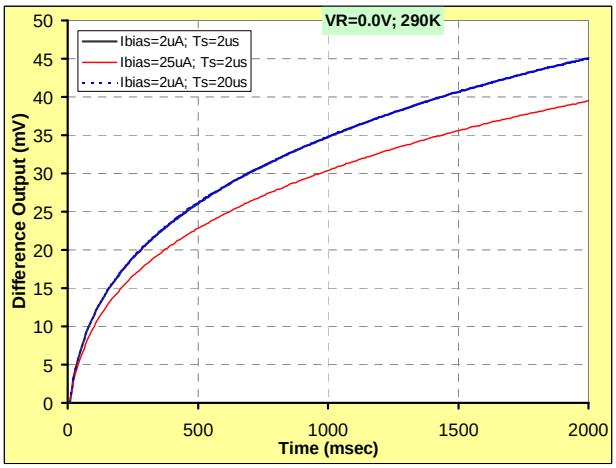

Figure 4: Measured data for different source-follower operating conditions

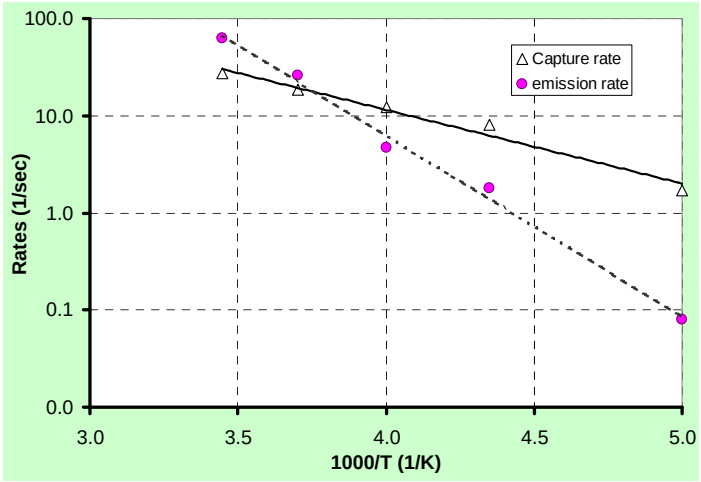

Figure 5: Arhennius plot of capture and emission rates